MAPPING THE CHROMOSPHERIC PLASMA TOPOGRAPHY THROUGH CHROMOSPHERIC OSCILLATIONS

Scott W. McIntosh[1,2] **and Bernhard Fleck**[3]

[1]Universities Space Research Association, CPSS, Seabrook, MD 20706.
[2]Laboratory for Astronomy and Solar Physics, NASA GSFC, Mailcode 682.3, Greenbelt, MD 20771. , Email: scott@grace.nascom.nasa.gov
[3]European Space Agency, Research and Scientific Support Department, NASA GSFC, Greenbelt, MD 20771. , Email: bfleck@esa.nascom.nasa.gov

ABSTRACT

Recent research has shown that understanding the physical nature of chromospheric oscillations hinges critically upon the understanding of the plasma structure in which they are formed and observed. To this end we discuss the mapping of the chromospheric plasma topography through the analysis of simultaneous SOHO/MDI and TRACE time-series observations through a combination of Fourier and Wavelet based analysis techniques. We are able to construct a picture of the chromospheric plasma and its interaction with the wave modes present. Such a picture will focus studies on topographic regions that will form a simulation test-bed for theories of mode-conversion, dissipation and wave heating in the solar chromosphere.

1. INTRODUCTION

The question still exists as to the exact evolutionary path, from generation to extinction, of the ubiquitous oscillations observed in the quiet solar chromosphere. The underlying goal of this quest is to assess whether or not there is a sufficient wave flux to supply energy, through some as yet unidentified mechanism, to the ambient chromospheric and coronal plasmas. In recent simulation (Rosenthal et al. 2002; Bogdan et al. 2002, 2003) and observational investigations (Judge et al. 2001; Krijger et al. 2001; McIntosh et al. 2001; McIntosh & Judge 2001; McIntosh & Smillie 2003) the plasma's magnetic topology, or "canopy", has been demonstrated to have a significant influence on the chromospheric oscillations. In this paper we will present a combination of results that provide a consistent interpretation of chromospheric oscillations and their symbiotic interplay with the plasma topography.

Much of the analysis presented in this paper is (necessarily) based on the accurate analysis of multi-wavelength, high cadence (typically 10-15 seconds) time-series observations of the chromospheric plasma. The Solar and Heliospheric Observatory (SOHO; Fleck et al. 1995) Michelson Doppler Imager (MDI; Scherrer et al. 1995) and Transition Region Explorer (TRACE; Handy et al. 1999) Joint Observation Programs (JOP) #72 and #97 were specifically designed to provide a complete physical picture of the chromospheric topography and oscillations. Through the combined analysis of high cadence, multi-wavelength imaging (and spectroscopic data when available) time-series data we are able to construct a consistent picture of the chromospheric plasma and its interaction with the wave modes present. We believe that such a picture will help focus studies on topographic regions that will form a simulation test-bed for theories of mode-conversion, dissipation and wave heating in the solar chromosphere.

2. DATA ANALYSIS

In this section we will discuss and highlight some of the data analysis methods that we have applied recently to study the interaction of chromospheric oscillations and the atmosphere in which they are observed. Our discussion will focus on the application of Fourier and Wavelet (see, e.g., Torrence & Compo 1998) transform based techniques of timeseries analysis and what details of the chromospheric plasma can be inferred from their application. As a specific example we will use the data from the September 22, 2000 (07-12 UT) run of JOP97 and limit our discussion to the analysis of the co-spatial and co-temporal SOHO/MDI line-of-sight magnetograms ($B_{||}$) and TRACE 1700Å UV continua timeseries. In the following sub-sections we will describe the data reduction process and analysis methods that are being applied to investigate the behavior and interaction of chromospheric oscillations and the plasma topography.

Before, we commence the description of the analysis methods used to mine the data we must first briefly discuss the construction of the TRACE and MDI timeseries. The first step in the analysis involves the co-alignment of the initial TRACE and MDI frames of the timeseries, providing the co-alignment of the magnetic field context with the TRACE data. Following that initial step we form data-cubes for the TRACE timeseries, D_{1700}(x,y,t), with each frame co-aligned with the previous one until all are co-aligned to that at t=0 with sub-pixel accuracy (Tarbell 2002, Private Communication, employing the TRACE Interactive Data Language routine "tr_get_disp_2d.pro",

see also McIntosh, Fleck & Judge 2003 for an application of this procedure). This critical image correlation process ensures that the data-cubes are as stable as possible to the effects of contamination from cross-talk in the signal produced by solar rotation.

2.1. Chromospheric Plasma Topography: Plasma-β

In an effort to build a picture of the chromospheric plasma topography we employ the simplest approach to extrapolate the magnetic field, a potential extrapolation[1], of the time-averaged MDI $B_{||}$ from a simple Fourier approach. Once the three dimensional field $B(x, y, z)$ is extrapolated from $B_{||}$(x,y,0) we compute the magnetic pressure $P_{\rm B}(x, y, z) = B_{||}(x, y, z)^2/8\pi$ and the plasma-β ($\beta \equiv P_{\rm g}/P_{\rm B}$; where $P_{\rm g}$ is the model gas pressure). We make use of the Vernazza et al. (1981, VAL3C) model values of $P_{\rm g}$ interpolated onto the same vertical scale as that of the magnetic field extrapolation.

Now, it is straightforward to estimate the height at which the plasma-β is of order unity, five say, in the two-dimensional TRACE field-of-view (FOV). This height we call, for the sake of brevity, the β transition height, or βTH. In the left-hand panel of Fig. 1 we show the colour-coded spatial variation of the βTH and, as a visual aid, we have added contours with a spacing of 0.25 Mm. Clearly, the presence of the sunspot and complex network/plage magnetic fields influence the spatial variation of the βTH.

2.2. Fourier Analysis

Title et al. (1992) noted the dearth of chromospheric oscillations in and around plage regions. Krijger et al. (2001) expanded upon this to include regions that are local to Quiet Sun network elements. To investigate the influence of the global plasma topography on the oscillations being observed we can perform a simple Fourier analysis to provide a number of diagnostic quantities. So, to search for locations where the oscillatory power drops in the TRACE bandpasses we decompose the datacubes D_{1700}(x,y,t) using a Fast Fourier Transform at each spatial pixel, so that we have

$$\hat{f}_{1700}(x, y, \nu) = \frac{1}{\sqrt{2\pi}} \int_{-\infty}^{\infty} D_{1700}(x, y, t) e^{-i\nu t} dt \ , \quad (1)$$

where $\hat{f}$ indicates that the new cube is a complex quantity. We have exchanged the time coordinate for a frequency coordinate and we have created equivalent cubes, $\hat{f}_{1700}(x, y, \nu)$, in frequency ν (units: mHz). By integrating the Fourier power spectrum from 3-8 mHz we can construct a map of broad-band oscillatory power and an example is shown on the right-hand side of Fig. 1. From this figure alone we can get a feeling, albeit a very rough one given that this is from a potential field extrapolation and a crude measure of oscillatory power, about the topographical form of the chromospheric "canopy" field, its connectivity and how it influences the passage of chromospheric oscillations.

[1]While more sophisticated extrapolations, using magneto-static equilibrium calculations (as done by Metcalf et al. 1995), for example, are appealing, not enough is known concerning the gas thermodynamics to make them useful, in this context.

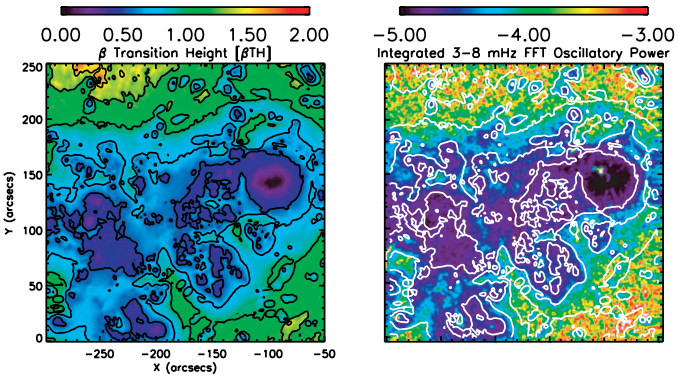

Figure 1. The plasma-β transition height (βTH; left panel) and the integrated 3-8 mHz oscillatory power in the 1700Å TRACE UV continuum (right panel). The contours shown are separated by 0.25 Mm. There is a strong correlation in these quantities.

A further diagnostic of canopy/chromospheric oscillations interaction is readily available from this simple Fourier analysis. We can compute the spatial variation of the TRACE bandpass phase-differences (McIntosh et al. 2003[2]) from the full spatial resolution complex frequency cube computed above. To compute the phase-difference spectrum we must first compute the cross-power spectrum $\hat{C}_{i,j}(x, y, \nu)$ for any two of the three bandpasses i and j, say. This is simply defined by

$$\hat{C}_{ij} = \hat{f}_{\lambda_i} * \hat{f}^{\dagger}_{\lambda_j}, \quad (2)$$

where $\hat{f}^{\dagger}$ is the complex conjugate of $\hat{f}$. The phase-difference spectrum $\Delta\phi_{ij}(x, y, \nu)$ is given by the argument ($\Delta\phi_{ij} \in [-\pi, \pi]$) of $\hat{C}_{ij}$, i.e.,

$$\Delta\phi_{ij}(x, y, \nu) = \tan^{-1}\left(\frac{\Im\{\hat{C}_{ij}(x, y, \nu)\}}{\Re\{\hat{C}_{ij}(x, y, \nu)\}}\right) . \quad (3)$$

The next step in our data analysis is then to compute the phase-difference spectra for the three bandpass combinations (1700-1600Å; 1700-1550Å; 1600-1550Å) and characterize the behavior spatially. That is, we have to measure the phase-difference change over a limited frequency range and one approach is to estimate/fit the gradient ($M_{\Delta\phi} = d(\Delta\phi_{ij})/d\nu$; units Degrees mHz^{-1}) of the phase-difference spectrum as a function of frequency. This gradient, $M_{\Delta\phi}$, is effectively proportional to the difference in bandpass formation heights (Δz_{ij}) and the reciprocal of the phase-speed (V_{phase}) of any perturbation present there, $M_{\Delta\phi} \approx \Delta z_{ij}/V_{phase}$ (e.g., Deubner & Fleck 1990). Unfortunately, this measure cannot be made at the full spatial resolution of TRACE and we must degrade the data to obtain gradient fits that have small enough errors[3] ($\leq \pm 1$ Degrees mHz^{-1}) without significantly smearing the spatial contrast. In this paper we

[2]This analysis includes the incorporation of the fact that the three bandpass images are not taken simultaneously, thus, the phase-difference spectra require a frequency-dependent shift to be calculated and applied.

[3]A full discussion of the methodology and error estimation in the computation of $M_{\Delta\phi}$ can be found in McIntosh et al. (2003); McIntosh & Fleck (2003).

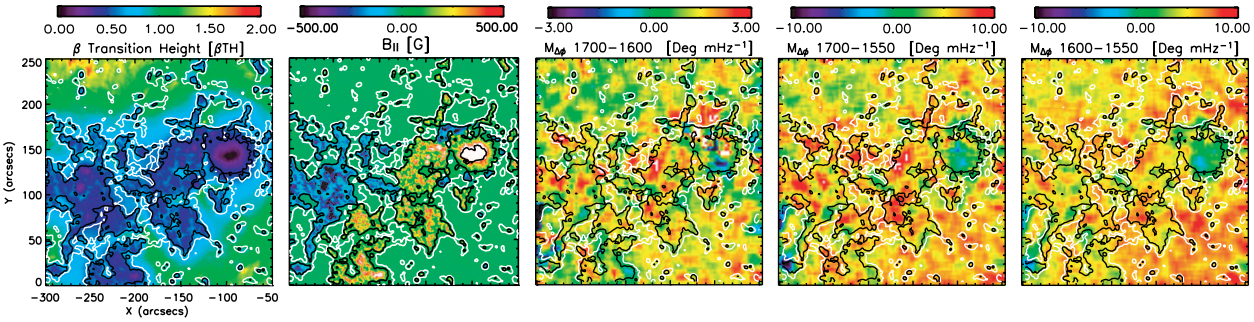

Figure 2. From left to right we show the βTH , the mean line-of sight MDI magnetogram and the three phase-difference gradient ($M_{\Delta\phi}$) 1700-1600; 1700-1550; 1600-1550Å for TRACE (5" × 5") "super-pixels". The contours shown mark the separation between the network ($B_{||} \geq 20$ Gauss; inside the black contours) and inter-network ($B_{||} \leq 10$ Gauss; outside the white contours) regions.

choose to use "super-pixels" that are 5" × 5" (or 10 × 10 TRACE pixels) in dimension. In Fig. 2 we show, from left to right, a comparison of the βTH , the time-averaged MDI magnetogram, and the maps of $M_{\Delta\phi}$ derived from the three TRACE bandpass pairs which, incidently, form a closed set (see, e.g., McIntosh & Fleck 2003). The spatial distribution of $M_{\Delta\phi}$ is not a clear diagnostic of the chromospheric topography and it appears that there is not a great deal of correlation between βTH and $M_{\Delta\phi}$ in any of the three cases available; except in the inter-network regions to the SE of the active complex and in the enhanced regions around the neutral-line dividing positive and negative polarity regions.

There are two mechanisms that contribute to the patterns in the derived $M_{\Delta\phi}$ maps :

- Variations in the phase speed of the specific magneto-atmospheric wave modes. Multi-dimensional magnetohydrodynamic simulations are the key to decoupling and understanding these wave-modes, as discussed in Rosenthal et al. (2002); Bogdan et al. (2002, 2003).
- Variations in the formation heights of the TRACE UV continua. The greater the degree of overlap, the smaller the value of $M_{\Delta\phi}$, as would most likely be the case in the network plasma. Conversely, in the farthest reaches of the internetwork plasma we might expect the least overlap of the bandpasses. In this case, detailed radiation transfer calculations, like those presented in Carlsson & Stein (2002), of these bandpasses are required to evaluate the exact degree of overlap for specific physical conditions.

Unfortunately, in regions where the threading magnetic topology is this complex the interpretation of $M_{\Delta\phi}$ derived solely from bandpass images is particularly fraught with ambiguity and we will discuss the interpretation of these maps below. We note that McIntosh et al. (2003) provided a quiet Sun example where the correlation of the chromospheric topography and $M_{\Delta\phi}$ is more straightforward.

2.3. Wavelet Transform Analysis

Much of the analysis performed on chromospheric oscillations to date has been Fourier based and assumes (by definition) that the observed wave modes are persistent spatially and temporally over the duration of the observation. Clearly, that is a highly idealized approach when it comes to the analysis of the spatially and temporally intermittent chromospheric oscillations which occur as small isolated "packets" of as little as one or two wave periods, switch off and wait for a measurable amount of time before restarting. We define a packet as a short-duration, multi-frequency packet of oscillations in the timeseries observations and it is precisely this behavior that makes the analysis of chromospheric oscillations naturally amenable to a multi-scale time-frequency wavelet transform analysis (see, e.g., Torrence & Compo 1998). This is a logical extension of the Fourier analysis discussed above which allows for a user-determined degree of localization in frequency and time (simultaneously) with relatively high accuracy in both dimensions. This characterization of the wave-packet behavior requires the knowledge of when packets statistically exist in a timeseries, how many packets there are over the duration of the timeseries, how long they last, how much time passes between packets and what the mean frequencies of the wave-packet oscillations are. We define these four quantities as the wave-packet "metrics" and in what follows we will examine their appearance in our test dataset.

Figure 3 illustrates the wave-packet metrics in the continuum timeseries observations. The position of the white asterisk in the top right thumbnail image marks the location of the *pixel* timeseries that is extracted for wavelet analysis and presented in panel a). At first glance this timeseries would seem to present an oscillation with a period of about 4 minutes that seems to be temporally intermittent with sizeable breaks from regular periodic oscillation. In Panel b) we show the wavelet power spectrum of this pixel timeseries and the regions of high wavelet power are clearly visible, especially those having greater than 95 % statistical confidence, i.e. those inside the black contours. Also shown in panel b) is the cone-of-influence (black cross-hatched area under the curve) marking the region of uncertainty caused by the finite length of the timeseries. The power contained within both of these contours defines one instance of a multi-frequency wave-packet.

In Panel c) we show the "global wavelet power spectrum" (GWPS, as defined by Torrence & Compo 1998) which

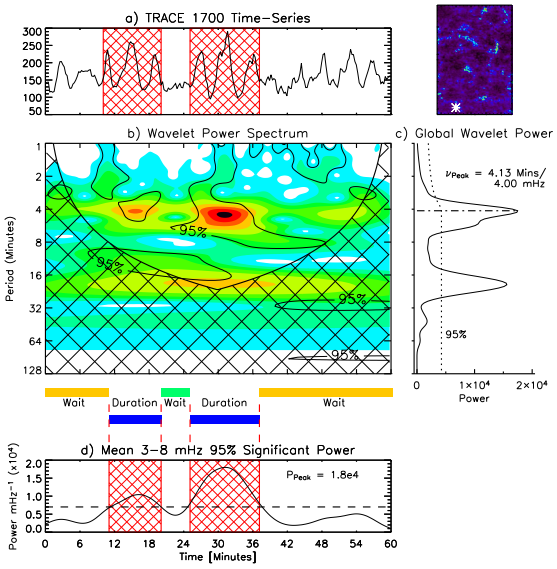

Figure 3. Example details of the wave-packet "metrics" used in this paper to characterize wave-packets in the TRACE UV continua timeseries observations. See description of the main details in the text.

is the mean wavelet power averaged over time and is the feature most comparable to the (significantly smoothed) Fourier power spectrum of the timeseries. From the GWPS we are able to define and measure the peak period 4.13 minutes (frequency of 4.00 mHz) of the wave-packets present. Similarly, the GWPS can be integrated over the same range of frequencies to obtain a measure of the average oscillatory power present in that spatial pixel (cf. Fig. 1). We note that the lower peak in the GWPS can be neglected since it belongs to packets that are predominantly within the cone-of-influence and are also not statistically significant, each of which is a criterion for rejection. The lowest panel in Fig. 3, panel d), shows the 3-8 mHz average wavelet power as a function of time. This is the object that allows us to measure the time-related metrics of the wave-packets present; the packet duration and the packet "wait-time" (the time between packets). The dashed line indicates the period-averaged 95% confidence level contours of panel b); the intersection of this line with the power curve marks the temporal boundaries of the wave-packets. These intersections are marked as finely cross-hatched areas on the panel which are similarly traced onto panel a). Clearly, there are two such "statistically significant" wave-packets in this particular hour long pixel timeseries.

In the center and right columns of Fig. 4 we demonstrate the spatial behavior of the wave-packet metrics beside those of the mean TRACE 1700Å continuum intensity (top left panel) and the MDI line-of-sight magnetic field strength $B_{||}$ (bottom left panel). The solid black and white contours, shown on each panel, mark the boundary between the network/plage and inter-network regions of the plasma, respectively, as was also illustrated in Fig. 2. Several features are immediately clear, as one might expect from the discussion above. The lower packet frequencies inside the network/plage regions are contained within these contours (center top panel). Similarly, in network regions there appear to be fewer wave-packets (top right panel) which is consistent with the fact that the wait time is significantly longer there (bottom right panel). Despite all of these relatively strong spatial correlations the wave-packet duration (center bottom panel) shows little to no dependence on where the packets are located, with the possible exception of the sunspot penumbra.

3. DISCUSSION

In what has been presented above we have seen that the spatial location of the region where the magnetic and hydrodynamic forces balance, i.e. where the plasma-β is of order unity, is critical to understanding the oscillatory signals that are observed. Tantalizingly enough, in the quiet Sun, this region lies in the mid-to-upper chromosphere at a point where we can meaningfully supply mass and energy to the corona (McIntosh et al. 2001). In addition, open and closed magnetic structures in the line-of-sight can alter and "quench" the chromospheric oscillations and UV intensities alike (see, e.g., McIntosh & Judge 2001). We have demonstrated some diagnostics that may allow us to discriminate between some of the many influences on chromospheric oscillations from generation to their eventual dissipation.

In Fig.5 we provide some illustrative cartoon visualizations of the plasma topography in axisymmetric strong and weak-field cases that can be readily compared to their two-dimensional counterparts presented previously by Gabriel (1976) and Peter (2001) (and others). These cartoons can be used to discuss the variation of the chromospheric oscillation diagnostics with the plasma topography as we have discussed them above. Note that the spatial (x-y) scales of each cartoon are different; with the weak-field case (lower left cartoon) represented with twice the spatial scale of the strong-field case (lower right cartoon). We assume that the vertical (z) scales are the same[4]. In each of the lower cartoons we show the field topology (multi-colored solid lines), the plasma-$\beta = 1$ iso-contour (transparent grey region), an estimate of the vertical position of the TRACE 1700Å continuum formation layer (green gridded surface) and the total atmospheric pressure (gas pressure + magnetic pressure) isobars which correspond to the topographic locations where 5-minute (solid thick black line), 4-minute (solid thick green line) and 3-minute (solid thick blue line) period waves would form the characteristic period of oscillation. The latter actually take the form of iso-surfaces of period but for the sake of clarity in these cartoons we have reduced them in dimension. Notice the topological differences in each cartoon, the horizontal spread of the field, and the net effect that the strength of the magnetic field plays in contributing to the lowering of the characteristic period iso-surfaces.

With these cartoons in mind we can illustrate possible explanations for some of the specific examples of topographic influence on the timeseries diagnostics shown :

∗ In Sect. 2.2 we discussed the role of Fourier methods and, in particular, phase-differences between time-

[4]In the strong field case the vertical scale is set in units of 1 Mm while the horizontal scale is of the order of 10 Mm.

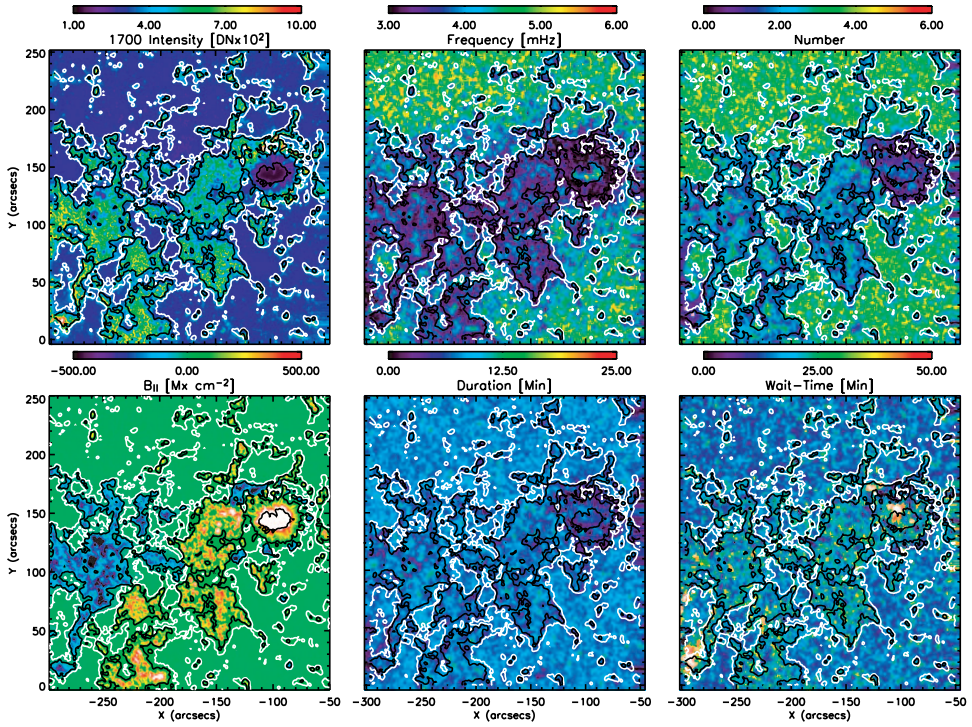

Figure 4. Wave-packet characteristics of the September 22, 2000 run of JOP97. Shown from top to bottom, left to right, are: the average 1700 Å intensity; the mean wave-packet frequency; wave-packet number; mean line-of sight MDI magnetogram; the wave-packet duration and the wave-packet wait-time. The contours shown mark the separation between the network and inter-network regions. Clearly, there are distinct differences between the network and inter-network regions in the TRACE field-of-view.

series as a diagnostic of the atmospheric topography. Unfortunately, in regions where the threading magnetic topology is this complex the interpretation of $M_{\Delta\phi}$ derived solely from bandpass images is particularly fraught with ambiguity without the aid of simulations and further spectroscopic observations. Indeed, the extension of the $M_{\Delta\phi}$ analysis to that of individual wavepackets is one which might provide further useful information, and is a subject of further investigation by the authors.

$*$ In Sect. 2.3 we have seen that the chromospheric oscillations observed are not persistent in time, lasting on average only a few periods before dying out and only to re-appear some time later and repeat. These oscillatory bursts are clearly identifiable as being short duration wave-packets making their analysis readily amenable to wavelet transforms. In characterizing the statistical, and spatial, behavior of these wave-packets we have defined metrics and shown that those metrics are dependent on the topography of the plasma being observed. We propose that the intersection of the TRACE 1700Å formation surface and the characteristic period iso-surface determines the frequency of wave packets that are observed and can explain some of the features observed in Fig. 4.

The work presented in this paper (and in McIntosh et al. 2001; McIntosh & Judge 2001; Rosenthal et al. 2002; Bogdan et al. 2002, 2003) demonstrates that understanding the position and role of the βTH may provide a critical link into the understanding of wave mode conversion, dissipation and ultimately the heating mechanism of the chromosphere. However, for the time being, the investigation of these effects will be limited to the complex, though not impossible (cf. Judge et al. 2001), combination of spectroscopic slit (SUMER) and passband imaging (TRACE) observations which lack Doppler velocity information. Indeed, that will be the case until we have a platform to perform some form of imaging spectroscopy, studying multiple line profiles simultaneously, spanning the vertical domain of the solar atmosphere in a less discrete fashion. This advance will accurately allow the diagnosis and mapping of the important region where the plasma-β is of order unity.

ACKNOWLEDGMENTS

SWM acknowledges the support of the GSFC SDAC and NASA's Living With A Star Program and the past support of a External Fellowship from the European Space Agency at GSFC and the European Solar Magnetometry Network (ESMN) under contract ERBFMRXCT980190.

REFERENCES

Bodgan, T. J., Rosenthal, C. S., Carlsson, M., et al. 2002, Astron. Nachr, **323**, 196

Bodgan, T. J., Rosenthal, C. S., Carlsson, M., et al. 2003, *In Press*, ApJS December 2003

Carlsson, M. & Stein, R. F. 2003, ApJ, **572**, 626

Deubner, F.-L. & Fleck, B., A&A, **228**, 506

Fleck, B., Domingo, V., Poland, A. I. 1995, *The SOHO mission*, Dordrecht: Kluwer

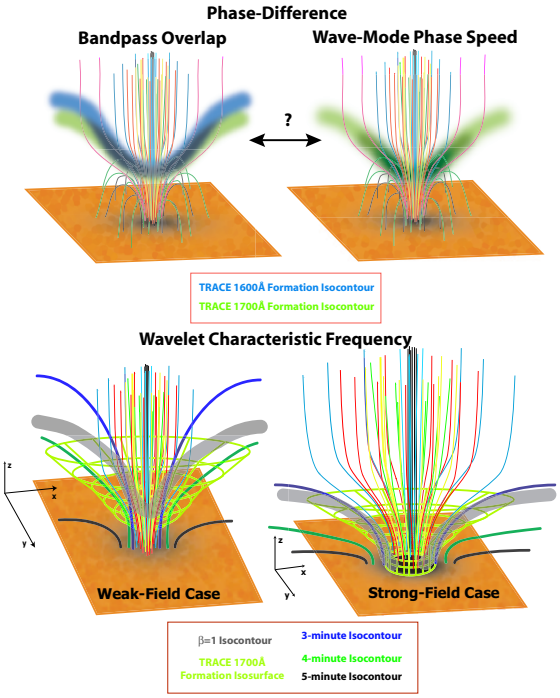

Figure 5. Some simple cartoons to discuss and explain some of the diagnostics and metrics discussed in the text and shown in Figs. 3, 4. The top pair of cartoons discuss the relative contribution to the phase-difference gradient ($M_{\Delta\phi}$) of bandpass overlapping and/or the phase-speed of any wave-modes present. More often than not, however, this pair are superimposed on one-another and cannot easily be disentangled. The lower pair of cartoons offer a pictorial explanation of the variation of wave-packet characteristic frequencies and how the interaction of the plasma topography (through the constant total pressure and βTH) and the TRACE bandpass formation height interact to influence what frequencies we see in, and where we observe, chromospheric oscillations.

Gabriel, A. H. 1976, Phil. Trans. R. Soc. Lond. A, **281**, 339

Handy, B. N., Acton, L. W., Kankelborg, C. C., Wolfson, C. J., Akin, D. J. et al. 1999, Solar Phys., **187**, 229

Judge, P. G., McIntosh, S. W. 1999, Solar Phys., **190**, 331

Judge, P. G., Tarbell, T. D., Wilhelm, K. 2001, ApJ, **554**, 424

Krijger, J. M., Rutten, R. J., Lites, B. W., et al. 2001, A&A, **379**, 1052

Lites, B. W., Chipman, E. G. & White, O. R. 1982, ApJ, **253**, 367

Metcalf, T. R., Jiao, L., McClymont, A. N., et al. 1995, ApJ, **439**, 474

McIntosh, S. W., Bogdan, T. J., Cally, P. S., et al. 2001, ApJ, **548**, L237

McIntosh, S. W., Judge, P. G. 2001, ApJ, **561**, 420

McIntosh, S. W., Fleck, B., Judge, P. G. 2003, A&A, **405**, 706

McIntosh, S. W., Smillie, D. G. 2003, Submitted ApJ (September 2003)

McIntosh, S. W., Fleck, B. 2003, *To appear in the proceedings of IAU Symposium 219.*

Peter, H. 2001, A&A, **374**, 1108

Rosenthal, C. S., Bodgan, T. J., Carlsson, M., et al. 2002, ApJ, **654**, 508

Scherrer, P. H., Bogart, R. S., Bush, R. I., Hoeksema, J. T., Kosovichev, A. G. et al. 1995, Solar Phys., **162**, 129

Title, A. M., Topka, K. P., Tarbell, T. D., et al. 1992, ApJ, **393**, 782

Torrence, C., Compo, G. P 1998, Bull. Am. Met. Soc., **79**, 61

Vernazza, J. E., Avrett, E. H. & Loeser, R. 1981, ApJS, **45**, 635

Wilhelm, K., Curdt, W., Marsch, E., et al. 1995, Solar Phys., **162**, 189